Canadian Chemical Transactions Year 2016 | Volume 4 | Issue 3 | Page 398-414

Research Article

DOI:10.13179/canchemtrans.2016.03.0330

Synthesis, Spectral (Uv-Vis, FT-IR and NMR), Molecular structure, NBO, HOMO-LUMO and NLO Analysis of Some 3t-pentyl-2r,6c-diarylpiperidin-4-one Semicarbazones

Mariadoss Arockia doss, Subramaniyan Amala, Govindasamy Rajarajan* and Venugopal Thanikachalam

Department of chemistry, Annamalai University, Annamalainagar 608 002, India

**Corresponding Author, Email: rajarajang70@gmail.com*

Received: *July 26, 2016* ***Revised:*** *September 8, 2016* ***Accepted:*** *September 18, 2016* ***Published:*** *October 2, 2016*

Abstract: 3*t*-pentyl-2*r*,6*c*-diarylpiperidin-4-one semicarbazones (**PDPSs**) have been synthesized and their Uv-Vis, IR, ^{1}H and ^{13}C spectra were recorded. The optimized geometric parameters (bond lengths, bond angles and dihedral angles) were in good agreement with the corresponding experimental values. Density functional theory assessment for the determination of vibrational wavenumber is examined, comparing the computed and experimental values. The hyperconjugative interaction energy ($E^{(2)}$) and electron densities of donor (i) and acceptor (j) bonds were calculated using NBO analysis. In addition, HOMO-LUMO, MEP and atomic charges of carbon, nitrogen and oxygen were calculated using B3LYP/6-311++G(d,p) level theory. Uv–Vis spectrum of **PDPSs** was recorded in different solvents in the region of 200–800 nm and the electronic properties such as excitation energies, oscillator strength, wavelengths were evaluated by time-dependent DFT (TD-DFT) approach. The polarizability and first order hyperpolarizability of the title molecule were calculated and interpreted.

Keywords: Semicarbazone; DFT; HOMO – LUMO energies; NLO.

1. INTRODUCTION

The piperidone and its derivatives are a class of nitrogen containing heterocycles that have received much attention because of their wide range of biological activities [1-5] as well as properties useful from the technological point of view [6,7]. Piperidin-4-one semicarbazones were also used as corrosion and oxidation inhibitors [8]. Therefore, importance of piperidin-4-one semicarbazone has strongly stimulated the investigation of computational properties available for these compounds. DFT calculations provide accurate results on systems such as large organic molecules [9]. Regardless of this fact, studies regarding the investigation of their conformation(s) and their electronic structure by computational techniques are lacking in the chemical literature [10,11]. Following our studies on the 3t-pentyl-2r,6c-diphenylpiperidin-4-one semicarbazone [12], we thought it could be of interest to extent these research to 3*t*-pentyl-2*r*,6*c*-diarylpiperidin-4-one semicarbazones (aryl = *p*-FC_6H_4 **(1)**, *p*-ClC_6H_4 **(2)**, *p*-BrC_6H_4 **(3)**, *p*-$CH_3C_6H_4$ **(4)**), Herein, we synthesized compounds **1-4** by condensing equimolar amounts of the respective piperidin-4-one and semicarbazide in methanol medium. The synthesised compounds

characterized by using Uv- vis, FT- IR and NMR point of view. In addition, we describe the study their preferred conformation(s) in gas phase by means of a computational approach. In the present study, DFT/ 6-311++G (d,p) level theory was used to determine the optimized geometry, vibrational wavenumber in the ground state, non-linear optical properties, HOMO–LUMO energies and Mulliken charges of the molecules. The Uv-Vis spectrum was calculated using TD-DFT/6-311++G(d,p) based on the optimized structure in gas phase and in solvents (chloroform and methanol). Furthermore, NBO analysis of **1-4** were performed in the same level of theories to determine the second order perturbation energy in terms of delocalization energy $E^{(2)}$.

2. EXPERIMENTAL DETAILS

2.1 Synthesis

3*t*-pentyl-2*r*,6*c*-diarylpiperidin-4-one was synthesized as per the procedure described in literature [13]. To a solution of 3t-pentyl-2r,6c-diarylpiperidin-4-one (0.01 mol) in 45 mL methanol and few drops of conc. HCl were added. Then, semicarbazide (previously dissolved in 20 mL methanol) solution (0.01 mol) was added drop wise with stirring. The reaction mixture was refluxed for 3 h on a heating mantle. After cooling, the solid product was filtered off and recrystallized from 20 mL methanol.

2.2 Spectral measurements

The Uv–Visible spectrum of compounds was recorded in SHIMADZU UV-1800 Uv–Visible Spectrophotometer at room temperature. The FT-IR spectrum of the synthesized **PDPSs** was measured in the range 4000-500 cm^{-1} on a AVATAR-330 FT-IR spectrometer (Thermo Nicolet) using KBr (pellet form). ^{1}H NMR spectrum was recorded at 400 MHz and ^{13}C NMR spectrum at 100MHz on a BRUKER model using $CDCl_3$ as solvent. Tetramethylsilane (TMS) was used as internal reference for all NMR spectra, with chemical shifts reported in δ units (parts per million) relative to the standard.

3t-pentyl-2r,6c- di(4-fluorophenyl) piperidin-4-one semicarbazone

Yield 80%; m.p.: 165-167 (ºC); MF: $C_{23}H_{28}F_2N_4O$; Elemental analysis: Calcd (%): C, 66.65; H, 6.81; N, 13.52; F, 9.49; O, 4.00; Found (%):C, 66.61; H, 5.74; N, 13.55; IR (KBr) (cm^{-1}): 3474 (υN-H), 3283(υNH_2semicarbazine unit), 2928 (υAr-CH), 2860 (υali-CH), 1695 (υC=O),1574 (υC=N), 1450 (υC=C), 1092 (υC-N), 1015-831 (aromatic C-H in-plane bending vibration),766-467 (aromatic C-H out of plane bending vibration); ^{1}H NMR(400 MHz, $CDCl_3$, δ,(ppm)): 8.39 (s,1H, NH), 7.00-7.07,7.36-7.52 (m, Ar-H), 6.08,4.09 (s, 2H, NH_2), 3.85 (dd,1H, H6) , 3.59 (d, 1H, H2), 2.91 (dd, 1H, H5eq), 2.40 (m, 1H, H3a), 2.09 (q, 1H, H5ax,), 1.08-1.64 (m, 8H, -CH2-), 0.80 (t, 3H, CH_3); ^{13}C NMR (100 MHz, $CDCl_3$, δ, ppm): 158.24 (C=O),151.12 C(4), 115.07-115.63, 128.18-129.55, 138.25-138.98 (Ar-C), 67.18 C(2), 60.09 C(6), 50.23 C(3), 36.50 C(5), 22.49-32.23 (-CH2-), 14.06 (CH_3).

3t-pentyl-2r,6c- di(4-chlorophenyl) piperidin-4-one semicarbazone

Yield 87%; m.p.: 162-164 (ºC); MF: $C_{23}H_{28}Cl_2N_4O$; Elemental analysis: Calcd (%): C, 60.97; H, 6.05; N, 12.93; Cl, 16.36; O, 3.69; Found (%):C, 61.74; H, 5.96; N, 12.56; IR (KBr) (cm^{-1}): 3466 (υN-H), 3269(υNH_2semicarbazine unit), 2947 (υAr-CH), 2924,2859 (υali-CH), 1694 (υC=O),1579 (υC=N), 1483 (υC=C), 1091 (υC-N), 1011-826 (aromatic C-H in-plane bending vibration),772-469(aromatic C-H out of plane bending vibration); ^{1}H NMR(400 MHz, $CDCl_3$, δ,(ppm)): 8.43 (s,1H, NH), 7.26-7.42 (m, Ar-H), 6.08,4.88 (s, 2H, NH_2), 3.84 (dd,1H, H6) , 3.59 (d, 1H, H2), 2.92 (dd, 1H, H5eq), 2.39 (q, 1H, H3a), 2.08 (t, 1H, H5ax,), 1.07-1.61 (m, 8H, -CH2-), 0.80 (t, 3H, CH_3); ^{13}C NMR (100 MHz,

$CDCl_3$, δ, ppm): 158.12 (C=O),151.74 C(4), 127.99-129.36, 133.49, 133.59,140.91, 141.59 (Ar-C), 67.20 C(2), 60.11 C(6), 50.08 C(3), 36.35 C(5), 22.51-32.23 (-CH2-), 14.06 (CH_3).

3t-pentyl-2r,6c- di(4-bromophenyl) piperidin-4-one semicarbazone

Yield 85%; m.p.: 170-172 (ºC); MF: $C_{23}H_{28}Br_2N_4O$; Elemental analysis: Calcd (%): C, 50.59; H, 5.02; N, 10.73; Br, 30.60; O, 3.06; Found (%):C, 50.48; H, 4.79; N, 10.62; IR (KBr) (cm^{-1}): 3464 (υN-H), 3276 (υNH_2semicarbazine unit), 2927 (υAr-CH), 2857 (υali-CH), 1695 (υC=O),1582 (υC=N), 1487 (υC=C), 1097 (υC-N), 1010-821 (aromatic C-H in-plane bending vibration),767 (aromatic C-H out of plane bending vibration); ^{1}H NMR(400 MHz, $CDCl_3$, δ,(ppm)): 8.28 (s,1H, NH), 7.27-7.35, 7.46-7.50 (m, Ar-H), 6.06,4.86 (s, 2H, NH_2), 3.83 (dd,1H, H6) , 3.58 (d, 1H, H2), 2.90 (dd, 1H, H5eq), 2.57 (t, 1H, H3a), 2.07 (q, 1H, H5ax,), 1.05-1.66 (m, 8H, -CH_2-), 0.80 (t, 3H, CH_3); ^{13}C NMR (100 MHz, $CDCl_3$, δ, ppm): 158.26 (C=O),150.72 C(4), 121.57,121.71,128.36-131.97,141.42,142.14 (Ar-C), 67.25 C(2), 60.14 C(6), 50.03 C(3), 36.24 C(5), 22.52-32.24 (-CH_2-), 14.07 (CH_3).

3t-pentyl-2r,6c- di(4-methylphenyl) piperidin-4-one semicarbazone

Yield 73%; m.p.: 148-150 (ºC); MF: $C_{25}H_{34}Br_2N_4O$; Elemental analysis: Calcd (%): C, 73.43; H, 8.22; N, 14.27; O, 4.08; Found (%):C, 72.13; H, 8.15; N, 13.12; IR (KBr) (cm^{-1}): 3474 (υN-H), 3264 (υNH_2semicarbazine unit), 3198,3025 (υAr-CH), 2924,2858 (υali-CH), 1698 (υC=O),1573 (υC=N), 1445 (υC=C), 1092 (υC-N), 1093-817 (aromatic C-H in-plane bending vibration), 767-723(aromatic C-H out of plane bending vibration); ^{1}H NMR(400 MHz, $CDCl_3$, δ,(ppm)): 7.80 (s,1H, NH); 7.15-7.33 (m, 8H, Ar-H); 6.09,4.80 (s, 2H, NH_2); 3.81 (d,1H, H6); 2.34 (6H, CH_3); 3.57 (d, 1H, H2), 2.78 (d, 1H, H5eq), 2.45 (t, 1H, H3a), 2.13 (t, 1H, H5ax,), 1.13-1.61 (m, 8H, -CH_2-), 0.84 (t, 3H, CH_3); ^{13}C NMR (100 MHz, $CDCl_3$, δ, ppm): 157.81 (C=O), 151.71C (4), 126.43-129.28, 137.47-140.26 (Ar-C), 67.65 C(2), 60.56 C(6), 50.02 C(3), 36.25 C(5), 22.53-32.29 (-CH_2-), 21.10 (CH_3); 14.05 (CH_3).

2.3 Computational studies

Structure optimizations of **PDPSs** were performed at the Density Functional Theory (DFT) level employing B3LYP/6-311++G(d,p) functional as implemented in the Gaussain 03W [14]. Vibrational analysis was carried out for all the minimized structures at the same level of theory. To investigate the reactive sites of the title molecules, the Mulliken and molecular electrostatic potential were evaluated. Moreover, in order to show nonlinear optical (NLO) activity of studied molecules, the dipole moment, linear polarizability and first order hyperpolarizability were obtained from molecular polarizabilities based on theoretical calculations. The electronic properties was calculated using TD-DFT/6-311++G(d,p) based on the optimized structure in gas phase and in solvents (chloroform and methanol). Also, the NBO population analysis and HOMO-LUMO on optimized structures are accomplished at B3LYP/6-311++G(d,p) level computation. The electronegativity (χ) were reported by Iczkowski et al.[15] is performed as $\chi = (E_{HOMO} + E_{LUMO})/2$. The global electrophilicity (ω)[16] is also calculated following the expression $\omega = (\mu^2/2\ \eta)$, where μ is the chemical potential ($\mu \approx (E_{HOMO} + E_{LUMO}) / 2$), and η is the chemical hardness $(E_{LUMO} - E_{HOMO})/2$)[17].

3. RESULTS AND DISCUSSION

3.1 Conformational analysis

The chair conformer of piperidine molecule is the most stable conformer [18,19]. Therefore, we neglected other conformations i.e. boat, envelope or twist boat because of their high energy. Piperidine

molecules show the equatorial disposition of N-H in chair conformer as the most stable one [20]. It is known from our previous study [12] that the E conformer of semicarbazone is more stable than the other possibilities. Therefore, in the present work we have focused on the E conformer for **PDPSs** molecules to clarify molecular structure, assignment of vibrational spectra, Uv-Vis spectra and HOMO–LUMO analysis, etc.

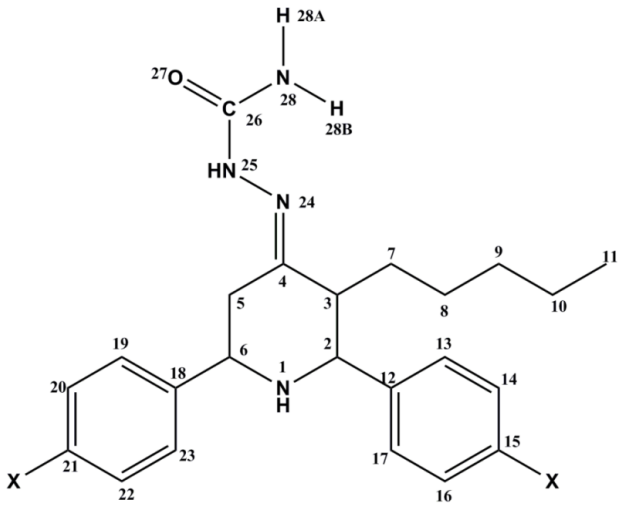

Compound	X
1	F
2	Cl
3	Br
4	CH_3

Figure 1. Numbering Pattern of **PDPSs**

3.2 Molecular geometry

The optimized structural parameters such as bond lengths, bond and dihedral angles of **PDPSs** were determined at B3LYP level theory with 6-311++G(d,p) basis set and are presented in Table 1 in accordance with the atom numbering scheme of the molecule shown in Figure 1. To the best of our knowledge, no single crystal X-ray crystallographic data of **PDPSs** has yet been reported. However, the theoretical results obtained are almost comparable with closely related molecules such as 3*t*-pentyl-2*r*,6*c*-diphenylpiperidine-4-one [21] and (*E*)-2-(hexan-2-ylidene)hydrazinecarboxamide [22]. The calculated C-C bond distance in the piperidine ring is in the range 1.509-1.582 Å by nearly coincides with experimental value 1.550- 1.56 Å [21]. The C2-N1 and C6-N1 bond nearly 1.461 Å by B3LYP, which is coincide with literature value ~1.461 Å [21].

The N25-C26-O27 and N28-C26-O27 angles are found to be around 120.00 and 125.00° (B3LYP). Difference within the values are as a result of inter- and intramolecular hydrogen bonding [12]. The lengthening of N28-H28A bond by about ~0.138 Å/B3LYP and shortening of C26-O27 bond by about ~0.031 Å (B3LYP) indicate the possibility of N28-H28A…..O27 hydrogen bonding [12]. Piperidine ring essentially adopts chair conformation, with all substituents equatorial as evident from the torsional angles [N1–C2–C3–C4 ≈ -55.00 and -51.99 and N1–C6–C5–C4 ≈ 52.00 and 54.81° by B3LYP and XRD, respectively. In the molecular optimized structure, the semicarbazone analogue is nearly planar with the dihedral angle (N24-N25-C26-N28) around 12.00° B3LYP and adopts an E configuration (Figure 2) with respect to the

C4=N24 bond [12]. Form the result we concluded that the E configuration is more stable than the other possibilities.

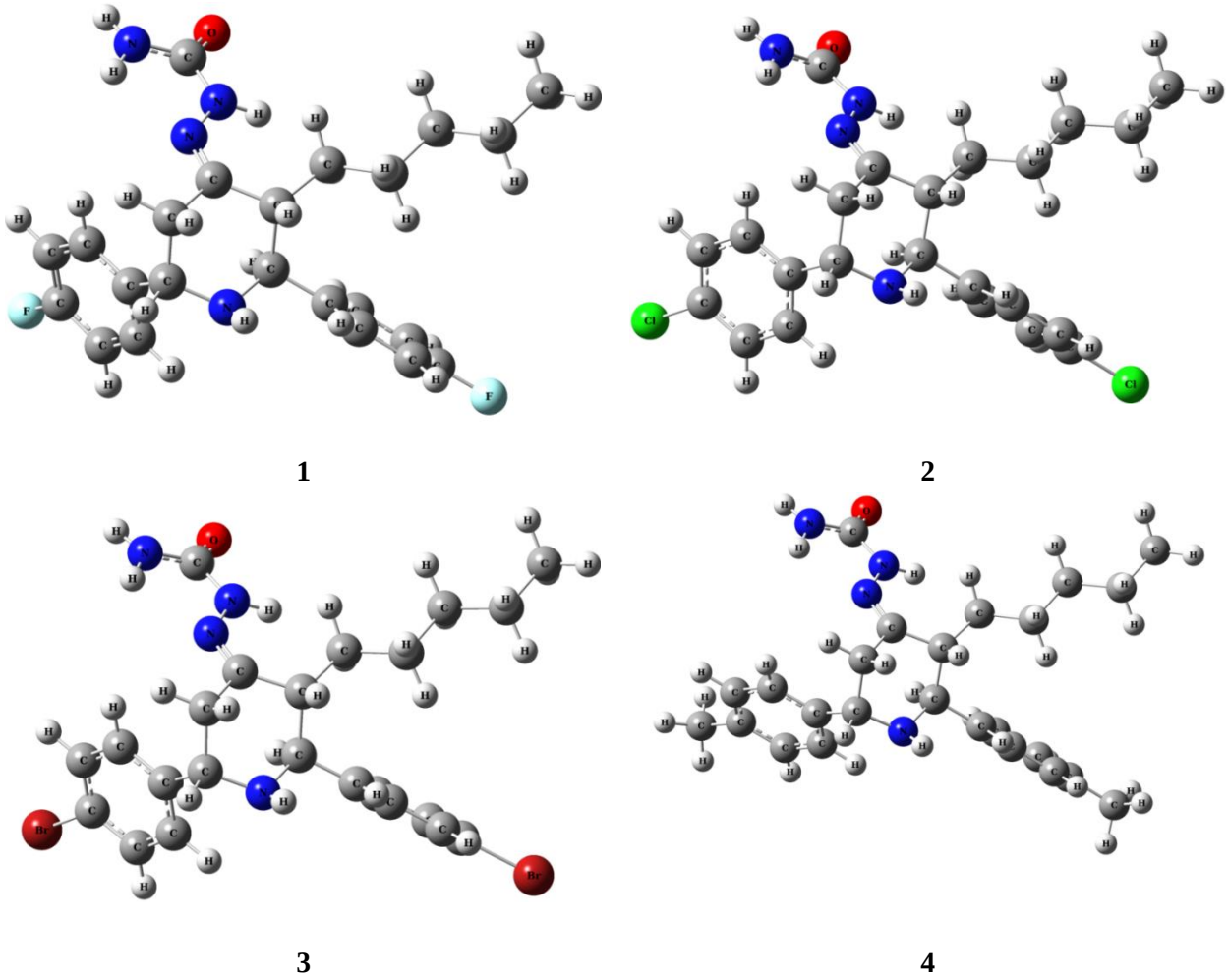

1 **2**

3 **4**

Figure 2. Optimized structures of **PDPSs**

3.3 IR spectral study

Vibrational frequency calculation was carried out on the optimized geometries of **PDPSs**. DFT hybrid B3LYP functional methods tend to overestimate the fundamental modes. Therefore, scale factor has to be used for obtaining a considerably better agreement with experimental data. Thus, the scale factor 0.9608 [12] has been uniformly applied to the DFT/ B3LYP method.

The important IR stretching frequencies of **1-4** are given in Table 2. In IR spectra, the presence of C =N stretching frequency around 1570 cm^{-1} confirms the hydrazone formation. The bands observed in the region of 3400–3473 cm^{-1} are due to N –H [23] stretching frequency of **PDPSs.** The band lie in the region 1685–1695 cm^{-1} are due to C=O stretching frequency of amide carbonyl group.

Table 1. Selected bond lengths, bond angles and dihedral angles of **PDPSs**.

Bond length (Å)	**1**	**2**	**3**	**4**	**XRD[a]**
C2-N1	1.471	4.4701	1.4711	1.471	1.471
C2-C3	1.5821	1.5826	1.5820	1.5816	1.550
C3-C4	1.5295	1.5302	1.5301	1.5269	1.526
C4-C5	1.5091	1.5098	1.5094	1.5701	1.506
C5-C6	1.5663	1.5556	1.5553	1.5606	1.532
C6-N1	1.4690	4.090	1.4093	1.4673	1.468
C4-N24	1.2836	1.2836	1.28358	1.2832	1.284
N25-C26	1.3991	1.997	1.998	1.975	1.367
C26-O27	1.2169	1.2167	1.2167	1.2176	1.249
C26-N28	1.3629	1.36201	1.3622	1.3648	1.341
N28-H28A	1.00495	1.00478	1.0049	1.0055	0.880
N28-H28B	1.00693	1.00662	1.00676	1.0081	0.870
C15-X	1.3508	1.7590	1.9171	1.5095	-
C21-X	1.3526	1.76125	1.9192	1.5095	-
Bond angle(^{o})					
N1-C2-C3	112.23	112.27	112.44	112.63	109.32
N1-C2-C12	109.14	109.05	108.86	108.88	108.71
N1-C6-C5	111.36	111.43	111.37	111.49	107.47
N1-C6-C18	110.14	110.00	110.09	111.34	111.22
N25-C26-O27	120.01	119.97	119.96	120.08	120.12
N28-C26-O27	125.34	125.37	125.39	125.31	1123.15
Dihedral angle(^{o})					
N1-C2-C3-C4	-55.65	-55.77	-55.36	-54.39	-51.99
N1-C6-C5-C4	52.07	51.99	52.21	51.10	54.81
N24-N25-C26-N28	13.00	12.82	12.69	11.29	12.90
N24-N25-C26-O27	-169.25	169.34	-169.49	-170.89	-178.06
N1-C2-C3-C12	172.69	172.54	173.07	174.47	178.04
H1-N1-C2-C12	56.07	56.86	55.80	50.28	-
H1-N1-C6-C18	-155.29	-155.74	-155.08	-150.87	-

a-Values are taken from Ref. 21 and 22

X= F, Cl, Br and CH_3 for **1, 2, 3** and **4**, respectively.

The aromatic C-H stretching [24, 25] is usually observed in the region 3150-3050 cm^{-1}. In our title compounds aromatic C-H frequency observed around 3090 cm^{-1}, whereas the aliphatic C-H stretching frequency is observed in the region 2924-2958 cm^{-1}. The band around 1090 cm^{-1} is due to C=C stretching of **PDPSs**. The in-plane and out-of-plane bending modes of title compounds are observed in the lower part of the spectra. Additional support for assignment of band of studied compounds was based on correlation between theoretical and experimental wavenumbers. As seen in from Figure 3 combined with Table 2 represents a very good linear correlation and standard deviation between theoretical and experimental wavenumbers of **PDPSs**.

Table 2. Experimental and calculated wavenumbers of **PDPSs**.

Assignment	**1**		**2**		**3**		**4**	
	Expt.	DFT	Expt.	DFT	Expt.	DFT	Expt.	DFT
ν_{N-H}	3473	3459	3466	3489	3468	3470	3400	3411
ν_{ArC-H}	3196	3196	3171	3175	3190	3193	3170	3178
ν_{C-H}	2927	2977	2924	2917	2927	2930	2958	2960
$\nu_{C=O}$	1695	1701	1694	1696	1685	1673	1686	1687
$\nu_{C=N}$	1573	1528	1579	1556	1569	1566	1508	1519
β_{C-H}	1450	1483	1483	1486	1457	1440	1421	1416
$\nu_{C=C}$	1092	1100	1092	1074	1089	1091	1020	1025
Γ_{C-H}	765	770	772	779	823	826	831	835
R^2	0.9996		0.9992		0.9997		0.9999	
SD	10.79		14.07		7.99		5.44	

ν- Stretching, β- in-plane bending, Γ-out-of-plane bending.
R-Correlation co-efficient, SD-Standard deviation

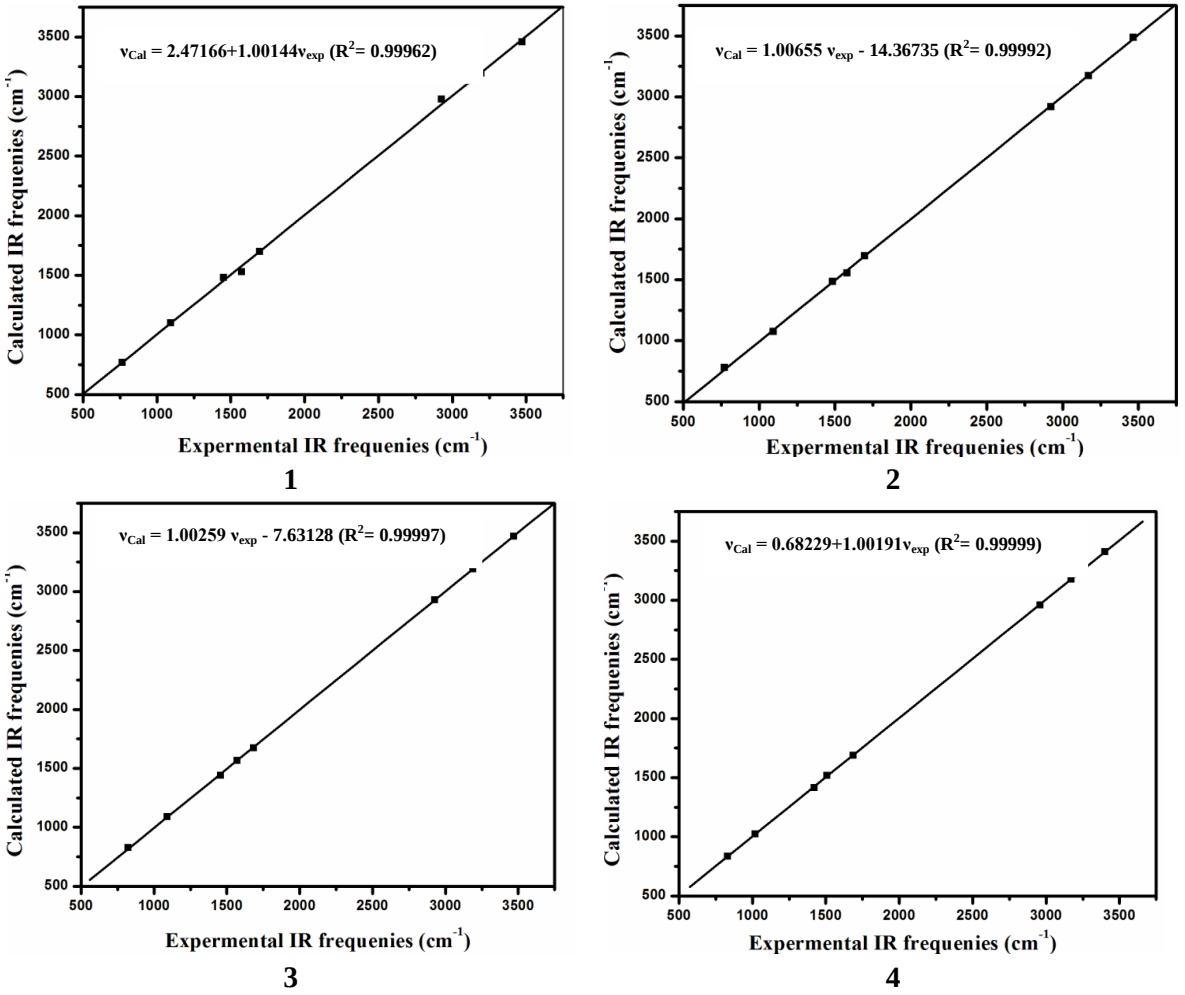

Figure 3. Correlation between experimental and calculated frequencies of **PDPSs**

3.4 NBO analysis

NBO analysis offers useful insights on the intramolecular delocalization and donor– acceptor interactions based on the second order interactions between filled and vacant orbitals. It is interesting to understand the important ground state stabilization interactions that make the molecules to be stable in ground state [26,27]. Hence NBO analysis has been carried out and the results are summarized in Table 3. This table lists the major second order perturbation interactions along with the corresponding donor and acceptor NBOs.

Table 3. Second order perturbation interactions obtained at B3LYP/6-311++G(d,p) from NBO calculations.

	Type	Donor (i)	ED/e	Acceptor(j)	ED/e	E^2 (kJ/mol)	E_j-E_i (a.u.)	Fi,j (a.u.)
	π - π *	C14 – C15	1.65887	C12 – C13	0.02511	85.35	0.30	0.070
	π - π *			C12 – C17	0.03451	81.71	0.29	0.068
1	n - π *	LP (1) N25	1.71901	C4 – N24	0.19292	123.97	0.29	0.085
	n - π *	LP (1) N28	1.78385	C26 – O27	0.30969	141.63	0.39	0.105
	n-σ*	LP (2) O27	1.84489	N25 – C26	0.08301	106.65	0.65	0.117
	π - π *	C18 – C19	1.65937	C20 – C21	0.38852	91.21	0.27	0.069
	π - π *	C22– C23	1.66684	C19 – C20	0.38852	89.66	0.27	0.069
2	n - π *	LP (1) N25	1.71745	C4 – N24	0.19377	125.39	0.29	0.085
	n - π *	LP (1) N28	1.78214	C26 – O27	0.31581	151.67	0.38	0.107
	n-σ*	LP (2) O27	1.84450	N25 – C26	0.06479	106.90	0.65	0.117
	π - π *	C18 – C19	1.65806	C20 – C21	0.38502	91.80	0.27	0.070
	π - π *	C23– C22	1.66359	C19 – C20	0.38502	89.12	0.27	0.069
3	n - π *	LP (1) N25	1.71660	C4 – N24	0.19444	126.36	0.29	0.085
	n - π *	LP (1) N28	1.78385	C26 – O27	0.06303	151.42	0.37	0.107
	n-σ*	LP (2) O27	1.84398	N25 – C26	0.08346	107.07	0.65	0.117
	π - π *	C18 – C23	1.65346	C19 – C20	0.33096	87.82	0.28	0.069
	π - π *	C19– C20	1.68193	C21 – C22	0.34513	86.53	0.29	0.070
4	n - π *	LP (1) N25	1.71599	C4 – N24	0.19302	124.60	0.29	0.085
	n - π *	LP (1) N28	1.78905	C26 – O27	0.30825	131.21	0.37	0.102
	n-σ*	LP (2) O27	1.84626	N25 – C26	0.08231	105.98	0.65	0.117

It is interesting to note that in all the molecules, the lone pair on oxygen atom participates in the stabilization of **PDPSs** through n- σ* interactions contributing nearly 106 kJ/mol towards stabilization. Yet the predominant stabilizing interactions in **PDPSs** show n-π* interactions arising from lone pair of nitrogen to the π* of adjacent C-O and C-N bonds which is dominant than the n- σ *. Overall the results highlight the importance of the incorporation of heteroatom towards the ground state stabilization of compounds.

3.5 Mulliken and MEP analysis

The calculation of atomic charges plays an important role in the application of quantum mechanical calculations to molecular systems. The Table 4 for **PDPSs** shows that the high positive charge in molecule is ~0.494 [C26], next charge value is ~0.117 [C4]. The positive regions are related to nucleophilic reactivity. The negative regions are located around the oxygen (O27) and nitrogen (N1, N24, N25 and N28) atoms which are related to electrophilic reactivity [28]. These data clearly show that **PDPSs** are the most reactive towards substitution reactions.

Table 4. Mulliken atomic charges of **PDPSs.**

Atom	**1**	**2**	**3**	**4**
C2	0.119259	0.119723	0.119615	0.11601
C3	-0.02936	-0.02712	-0.02575	-0.03203
C4	0.11799	0.117071	0.117044	0.109206
C5	0.056336	0.057733	0.05768	0.065986
C6	0.096957	0.093489	0.098264	0.100019
N1	-0.17372	-0.17148	-0.17282	-0.18022
C18	-0.13011	-0.11859	-0.11847	-0.09685
C12	0.016004	0.013156	0.011426	-0.00085
N24	-0.22996	-0.22982	-0.22946	-0.22924
N25	-0.0826	-0.08239	-0.08275	-0.08397
C26	0.491628	0.493786	0.493042	0.494056
N28	-0.00784	-0.00731	-0.00728	-0.00857
O27	-0.39147	-0.39023	-0.39028	-0.39556
X15	-0.23057	-0.0664	-0.02041	0.100977
X21	-0.2359	-0.07658	-0.03248	0.090763

X= F, Cl, Br and CH_3 for **1, 2, 3** and **4**, respectively.

Molecular electrostatic potential (MEP) is a useful descriptor used to visualize the electrophilic or nucleophilic reactive sites of molecular system [28], and to display the electrostatic potential regions in terms of color grading. In MEP map, different values of the electrostatic potential are represented by different colors: red and blue represents the regions of the most negative and positive electrostatic potential whereas green represents the region of zero potential. Potential increases in the order: red < orange < yellow < green < blue. The positive regions are placed around all hydrogen atoms attached with the nitrogen, which are related to nucleophilic reactivity [28].

The negative regions are located around the oxygen (O27) and nitrogen (N1, N24, N25 and N28) atoms. As shown in Figure 4, the negative and positive potential sites are around the electronegative (oxygen and nitrogen) atoms and the hydrogen atoms respectively, while the remaining species are surrounded by zero potential. As we conclude from this our title molecules are ready for both electrophilic and nucleophilic reactions.

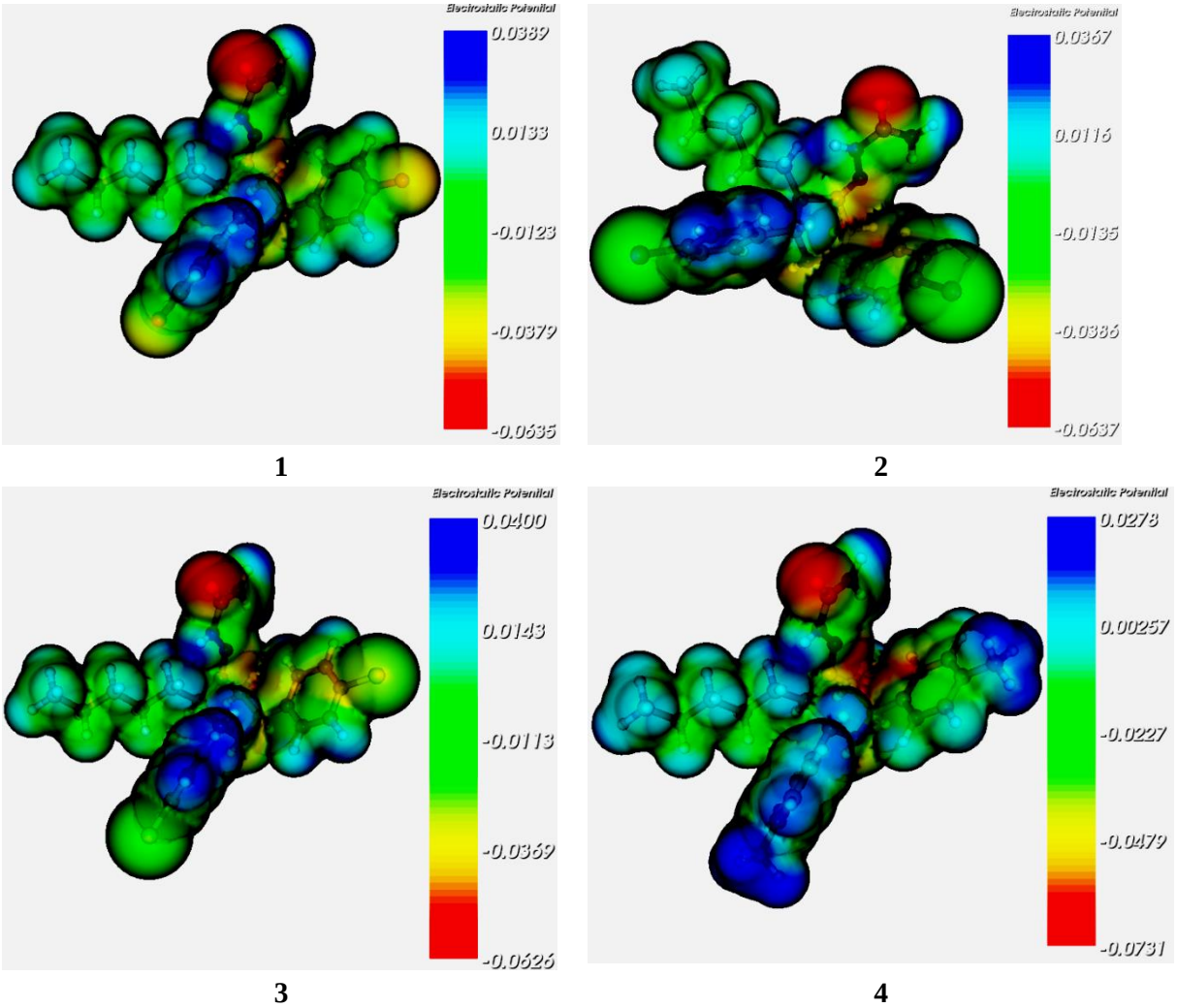

Figure 4. MEP diagram of **PDPSs.**

3.6 Ultraviolet spectroscopy

On the basis of the equilibrium geometries optimized at the B3LYP/6-311++G(d,p) level, absorption properties for the studied molecules were investigated by TDDFT method using same level theory. Then, the experimental and calculated wavelength (λ_{max}), the corresponding oscillator strength (*f*), electronic excitation energies and the transition nature are listed in Table 5. It can be found that the computed λ_{max} values of studied molecules are in good agreement with the experimental values.

The wavelengths of maximum absorption showed the red shifted behavior for all the molecules as compared to the computed values of **PDPSs**. As results shown in Table 5 and combined with Figure 6, it indicate that the absorption peaks are around 295 and 250 nm, and the main transitions appear around 305 nm for molecule **4**, which have methyl group substituted at 15 & 21-sites of the phenyl core. Moreover, the absorption peaks of the four molecules show obvious blue shifts in chloroform relative to the methanol solvent, which are around 280 and 245 nm. As seen from Table 5, for all the studied molecules, the main transitions with the strongest oscillator strength are assigned as HOMO-LUMO in absorption

process. In the meantime, it can be seen from Table 5 that the electron transition from HOMO - LUMO+ 1 and HOMO -LUMO+ 2 also makes some contributions in the absorption process.

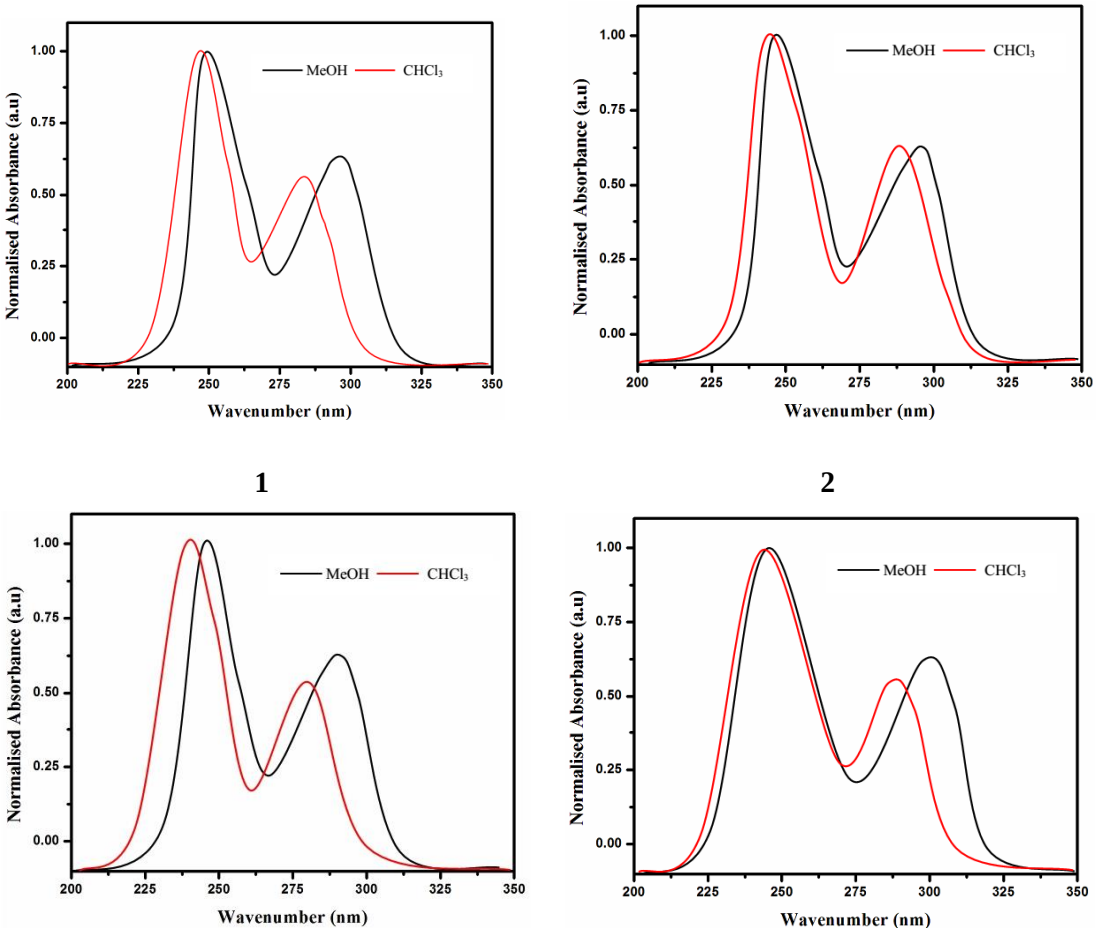

Figure 6. The experimental absorption spectrum of **PDPSs**.

3.7 Frontier molecular orbital analysis

The frontier molecular orbitals play an important role in the electric and optical properties, as well as in chemical reactions, Uv–Vis and fluorescence spectra [29, 30].The contour surfaces of the frontier molecular orbitals for each molecule are drawn in Figure 7. In the **PDPSs**, the electron cloud distribution in HOMO is piperidine ring and semicarbazone unit, but the contribution of molecular fragment to LUMO are mainly from the semicarbazone unit and phenyl group at C-2 position. The difference of the charge separation between the HOMO and LUMO of those structures plays important role in the internal charge transfer (ICT). Furthermore, energy diffrance between HOMO and LUMO of compounds **1-4**, which is due to different substituent at 15 & 21- sites of the phenyl core.

Table 5. Computed and experimental absorption maxima (λ_{max}, nm), Oscillator strength (*f*) and electronic excitation energies (E, eV) of **PDPSs**.

Molecule	State	Cal. λ_{max}(nm)	Expt. λ_{max}(nm)	Osicillator Strength (*f*)	E(eV)	Transition nature (%)
1	Gas phase	285.86		0.0657	4.3372	H→L (95)
		257.67		0.0127	4.8123	H→L+1 (90)
		247.65		0.0098	4.9357	H→L+2 (93)
	Methanol	294.57	296.00	0.0761	4.2095	H→L (96)
		256.13	249.00	0.0162	4.8412	H→L+1 (93)
		250.34		0.0139	4.9532	H→L+2 (90)
	Chloroform	290.14	298.00	0.0572	4.2737	H→L (96)
		255.24	247.00	0.0146	4.8581	H→L+1 (94)
		249.67		0.0123	4.9665	H→L+2 (91)
2	Gas phase	294.54		0.0742	4.2099	H→L (95)
		257.38		0.0215	4.8177	H→L+1 (94)
		250.12		0.0184	4.9576	H→L+2 (90)
	Methanol	296.45	295.00	0.0489	4.1828	H→L (93)
		258.84	245.00	0.0204	4.7906	H→L+1 (93)
		251.34		0.0196	4.9335	H→L+2 (92)
	Chloroform	285.09	287.00	0.0694	4.2021	H→L (93)
		249.28	245.00	0.0198	4.9743	H→L+1 (95)
		247.54		0.0143	5.0092	H→L+2 (92)
3	Gas phase	284.31		0.0564	4.3614	H→L (96)
		248.81		0.0185	4.9837	H→L+1 (94)
		247.45		0.0193	5.0111	H→L+2 (91)
	Methanol	289.93	288.00	0.679	4.2768	H→L (95)
		245.84	244.00	0.0154	5.0445	H→L+1 (90)
		243.75		0.137	5.0871	H→L+2 (92)
	Chloroform	281.79	280.00	0.1162	4.4004	H→L (95)
		250.15	240.00	0.0168	4.9570	H→L+1 (92)
		247.73		0.0120	5.0054	H→L+2 (91)
4	Gas phase	286.55		0.0735	4.3268	H→L (93)
		246.99		0.091	5.0204	H→L+1 (91)
		243.53		0.0183	5.0917	H→L+2 (90)
	Methanol	298.59	305.00	0.0537	4.3273	H→L (94)
		249.74	247.00	0.0189	4.9651	H→L+1 (90)
		245.45		0.0143	5.0519	H→L+2 (92)
	Chloroform	287.44	289.00	0.0671	4.3139	H→L (93)
		249.53	245.00	0.0146	4.9693	H→L+1 (95)
		247.75		0.0123	5.0050	H→L+2 (92)

Table 6. Calculated energy values (eV) of **PDPSs** in gas phase

DFT/B3LYP/6-311++G(d,p)	**1**	**2**	**3**	**4**
E_{total} (Hartree)	-1387.57	-2108.3	-6336.14	-1267.77
E_{HOMO}	-6.13	-6.21	-6.20	-5.89
E_{LUOMO}	-1.00	-1.12	-1.13	-0.68
$E_{LUMO-HOMO}$	5.13	5.09	5.07	5.21
E_{HOMO-1}	-6.69	-6.76	-6.67	-6.42
$E_{LUOMO+1}$	-0.80	-0.78	-1.01	-0.54
$E_{(LUMO+1)-(HOMO+1)}$	5.90	5.98	5.66	5.88
Electrinegativity(χ)	-3.56	-3.67	-3.66	-3.28
Hardness(η)	2.57	2.55	2.54	2.61
Electrophilicity index(ψ)	2.48	2.64	2.65	2.07
Softness(s)	144.24	145.45	145.91	142.08

As seen from Table 6, that the bromine containing aromatic substituent does play a role on the orbital distribution (HOMO and LUMO) and also has a direct influence on the electron density difference for the stabilizing ICT process. In this sense, it seems that the selection of a bromine containing substituent has a beneficial effect among the designed candidate. As a result, the trend of ΔE gap of inspected compounds becomes **4** > **1** > **2** > **3**. We can observe from this Table 6, the introduction of different substituent at 15 & 21- sites of the phenyl core significantly change the ΔE value.

Chemical hardness is related with the stability and reactivity of a chemical system, it measures the resistance to change in the electron distribution or charge transfer. In this sense, chemical hardness corresponds to the gap between the HOMO and LUMO. The larger the HOMO–LUMO energy gap, the molecule is harder and more stable/less reactive. Table 6 contains the computed chemical hardness values for compounds **1-4**. By analyzing the results, it can be seen that **4** is harder and less reactive than the other compounds.

The trend in electronic chemical potential for the compounds are 4 > 1 > 2 > 3. The greater the electronic chemical potential, then the compound is more stable or less reactive than the other compounds. Results of chemical hardness and electronic chemical potential of PDPSs showed that 4 are harder and less reactive than 1-3. Electrophilicity index measures the propensity or capacity of a species to accept electrons [31]. It is a measure of the stabilization in energy after a system has accepted additional amount of electronic charge from the environment. When comparing the PDPSs, the electrophilicity value of 4 (2.06 eV) is a stronger nucleophile than the 1-3. Results from Table 6, 4 shows that the strongest nucleophile whereas 3 shows that the strongest electrophile.

3.8 Non-linear optical activity

Organic materials with commutable NLO responses are sought for optoelectronic applications such as molecular-scale memory devices with multiple storage and nondestructive reading capacity [32]. A large variety of NLO switches exhibiting large changes in the first order hyperpolarizability (β). Some

quantum chemical descriptors which are total static dipole moment (μ), the mean polarizability (α), the anisotropy of the polarizability (Δα) and first order hyperpolarizability (β) have been used for explaining the NLO properties in many computational studies [32]. In this context, the design of NLO switches shows that molecules computed for their first order hyperpolarizability by alternate their substitution at 15 and 21- sites in phenyl core. The quantum chemical descriptors calculated from the Gaussian output have been explained in earlier work [33]. NLO properties increase with increasing the mean polarizability, anisotropy of the polarizability and first order hyperpolarizability.

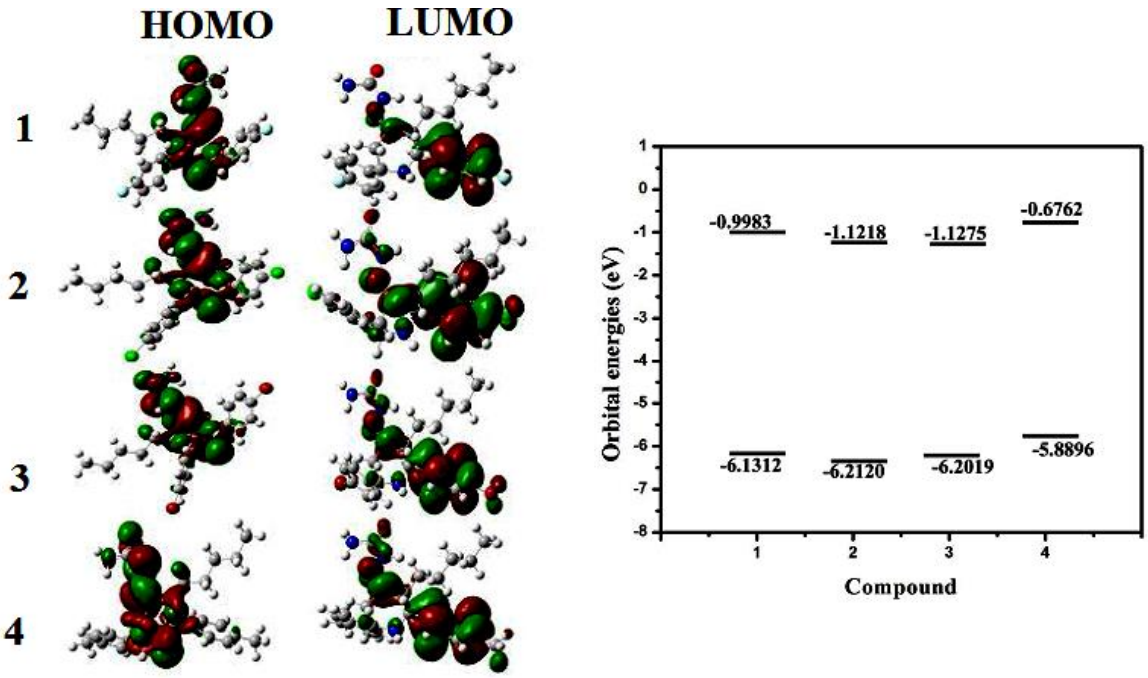

Figure 7. Molecular orbitals and energies for the HOMO and LUMO in gas phase.

Table 7. Non-linear optical properties of **PDPSs** calculated using B3LYP method using 6-311++G (d,p) basis set.

NLO behavior	**1**	**2**	**3**	**4**
Dipole moment(μ) D	4.86	5.14	5.05	4.59
Mean polarizabilty (α) x10^{-23} esu	2.75	3.01	3.15	2.67
Anisotropy of the Polarisabiltiy (Δα) x10^{-24} esu	3.65	4.21	4.64	4.87
First order polarizabilty (β_0) x10^{-30} esu	0.89	1.17	2.02	0.80

As the results mentioned previously [10,12], it can be reasonably predicted that the 3*t*-pentyl-2*r*,6*c*-diphenylpiperidin-4-one semicarbazone (**PDPOSC**) [12] may have significant nonlinear

optical property. Herein, on the basis of the **PDPOSC**, a series of new molecules possessing nonlinear optical property are designed which includes F, Cl, Br and methyl groups at 15 & 21- sites of the phenyl core. According to **Table 7**, all values of each mentioned molecules are greater than their urea values. Therefore, NLO properties of our compounds are better than urea. Results from Table 7, the general ranking of NLO properties should be as follows: **3** > **1** > **1** > **4**. With results in hand, molecule **3** is the best candidate for NLO properties. To sum up, it can be concluded that the presence of an electron donating group (methyl) in the *para* position at the phenyl ring contributes to decrease the dipole moments, mean polarisability and first order hyperpolarizability of the **PDPSs** probably because of an inductive competition between the methyl and the electronic density available in the molecule. The reverse trend is observed for mean anisotropy of the polarizability.

4. CONCLUSION

Results from in hand, piperidone ring adopts chair conformation with equatorial orientation of substituent at C3, C3, C6 and semicarbazone analogue adopts an E configuration with respect to C4=N24. The theoretically constructed FT-IR spectra coincide with the experimentally observed FT-IR spectrum. The **PDPSs** shows the n-σ* contributing energy amounts nearly 106 kJ/mol, which we treat as the evidence of the stabilization of compounds in ground state. In addition, Mulliken charge and MEP analysis predicts the most reactive parts in the molecule. The longest wavelength absorption corresponds to the excitation to the lowest singlet excited state, where the electronic transitions nature corresponds exclusively to the promotion of an electron from HOMO - LUMO in **PDPSs**. The result of molecular orbital composition analysis revealed for **PDPSs**, that the ΔE gap could be lowered upon modifying the 15 & 21- sites of the phenyl core. Among this, compound **3** is the best candidate for the stabilizing ICT process. Another conclusion of the paper is the calculated first hyperpolarizability and compare with reported values of similar derivatives and the **3** is a strong candidate for future studies of nonlinear optics.

ACKNOWLEDGMENTS

One of the authors, Dr. G. Rajarajan is thankful to UGC [F. No. 42-343/2013 (SR)] for providing funds to this research study. Mr. M. Arockia doss is thankful to UGC for providing fellowship. The authors also wish to thank Dr. N. Jayachandramani, former Head, Department of Chemistry, Pachaiyappa's college, Chennai-30.

REFERENCE

[1] Ramalingam, C.; Park,Y.T.; Kabilan, S. Synthesis, stereochemistry and antimicrobial evolution of substituted piperidine-4-one oxime ethers. *Eur. J. Med. Chem*. **2006**, *41*, 683-696.

[2] Balasubraanian, S.; Aridoss, G.; Parthiban, P. Synthesis and biological evalution of novel benzimidazol/benzoxazolylethoxypiperidone oximes. *Biol. Pharm. Bull*. **2006**, *29*, 125-130.

[3] Murugesan, S.; Perumal, S.; Selvaraj, S. Synthesis, stereochemistry, and antimicrobial activity of 2,6-diaryl-3-(arylthio)piperidin-4-ones. *Chem. Pharm. Bull*. (Tokyo) **2006**, *54*, 795-801.

[4] M.X. Li.; C.L. Chen.; C.S. Ling.; J. Zhou.; B.S. Ji.; Y.J. Wu.; J.Y. Niu. Cytotoxicity and structure–activity relationships of four α-N-heterocyclic thiosemicarbazone derivatives crystal structure of 2-acetylpyrazine thiosemicarbazone. *Bioorg. Med. Chem. Lett.* **2009**, *19*, 2704-2706.

[5] Sethukumar, A.; Udhaya Kumar, C.; Agilandeshwari, R.; Arul Prakasam, B. Synthesis, stereochemical, structural and biological studies of some 2,6-diarylpiperidin-4-one N-(4') cyclohexyl thiosemicarbazones. *J. Mol. Struct*. **2013**, *1047*, 237-248.

[6] Jayabharathi, J.; Thanikachalam V.; Padamavathy, M.; Srinivasan, N. Synthesis and physicochemical studies of some novel picrate derivatives, *Spectrochim. Acta, Part A*. **2011**, 81, 380-389.
[7] Jayabharathi, J.; Thanikachalam V.; Padamavathy, M.; Venkatesh Perumal, M. Photophysical Properties of Novel Picrate Derivatives – Solvent Effect, *J. Fluoresc*. **2012**, *22*, 269-279.
[8] Ravikumar, L.; Rathika, G.; Punitha, R. Study Of The Protection Of Mild Steel Corrosion With Piperidin -4-One And Its Semicarbazones. *Int. J. Eng. Res. Tech*. **2013**, *2*, 3137-3143.
[9] Subashchandrabose, S.; Saleem, H.; Erdogdu, Y.; Rajarajan, G.; Thanikachalam, V. 3-pentyl-2,6-diphenylpiperidin-4-one. *Spectrochim Acta Part A*. **2011**, *82*, 260-269.
[10] Dhandapani, A.; Manivarman, S.; Subaschandrabose, S.; Saleem,H. (E)-1-(3-methyl-2,6-diphenyl piperidin-4-ylidene) semicarbazide. *J. Mol. Struct*. **2014**, *1058*, 41-50.
[11] Velraj, G.; Soundharam, S.; Sridevi, C. Structure, vibrational, electronic, NBO and NMR analyses of 3-methyl-2,6-diphenylpiperidin-4-one (MDPO) by experimental and theoretical approach. *J. Mol. Struct*. **2014**, *1060*, 156-165.
[12] Arockia doss, M.; Savithiri, S.; Rajarajan,G.; Thanikachalam,V.; Saleem, H. Synthesis, spectroscopic (FT-IR, FT-Raman, UV and NMR) and computational studies on 3*t*-pentyl-2*r*,6*c*-diphenylpiperidin-4-one semicarbazone. *Spectrochim Acta Part A*. **2015**, *148*, 189-202.
[13] Savithiri, S.; Rajarajan, G.; Srividhya, V.; Jijesh, J.; Thanikachalam, V.; Jayabharathi, J.; Arockia doss, M. Synthesis, spectral and structure activity relationship studies of substituted 3t-pentyl-2r, 6c–diarylpiperidin-4-ones and their corresponding oxime derivatives. *Can. Chem. Trans*. **2014**, *2*, 201 -220.
[14] Frisch, M.J. et al., Gaussian 03, Revision E.01, Gaussian Inc, Wallingford, CT, 2004.
[15] Iczkowski, R.P.; Margrave, J.L. Electronegativity. *J. Am. Chem. Soc*. **1961**, *83*, 3547-3551.
[16] Parr, R. G.; Szentpaly, L; Liu, S. Electrophilicity Index. *J. Am. Chem. Soc*. **1999**, *121*, 1922-1924.
[17] Parr, R. G.; Pearson, R. G. Absolute Hardness: Companion Parameter to Absolute Electronegativity. *J. Am. Chem. Soc*. **1983**, *105*, 7512-7516.
[18] Manimekalai A.; Sivakumar, S. Synthesis, spectral and conformational studies of some N-arylsulfonyl-*t*(3)-isopropyl-*r*(2),*c*(6)- diarylpiperidin-4-ones. *Magn. Reson. Chem*. **2011**,*49*, 830-834.
[19] Jayabharathi, J.; Thangamani, A.; Balamurugan, S.; Thiruvalluvar A.; Linden, A. t-3-Benzyl-r-2,c-6-bis-(4-methoxy-phen-yl)-piperidin-4-one. *Acta Cryst*. **2008**, E*64*, o1181.
[20] Ravichandran, K.; Sethuvasan,S.; Thirunavukarasu, K.; Ponnuswamy, S.; Ponnuswamy, M. N. 3-Isopropyl-2,6-bis-(4-meth-oxy-phen-yl)-piperidin-4-one. *Acta Cryst*. **2012**, E*68*, o2453.
[21] Gayathri, J.; Jayabharathi, J.; Rajarajan, G.; Thiruvalluvar, A.; Butcher, R.J. t-3-Pentyl-r-2,c-6-diphenyl-piperidin-4-one. *Acta Crystallogr*. **2009**, E*65*, o3083.
[22] Chia, T.S.; Quah, C.K.; Ooi, C.W.; Garudachari, B.; Isloor, N.A.; Isloor, A.M.; Fun, H.K. Syntheses, Crystal Structures and Antimicrobial Studies of Two New Semicarbazone Derivatives. *J. Chem. Crystallogr*. **2014**, *44*, 51-56.
[23] Socrates, G. Infrared and Raman Characteristic Group Frequencies. Wiley, New York, 2001.
[24] Gussoni, M.; Castiglioni, C.; Ramos, M.N.; Rui, M.; Zerbi, G. Infrared intensities: from intensity parameters to an overall understanding of the spectrum. *J. Mol. Struct*. **1990**, *224*, 445-470.
[25] Pavia, D.L.; Lampman, G.M; Kriz, G.S.; Vyvyan, J.R. Spectroscpoy. Cengage Learing, New York, 2008.
[26] Szafran, M.; Komasa, A.; Adamska, E.B. Crystal and molecular structure of 4 carboxypiperidinium chloride (4-piperidinecarboxylic acid hydrochloride). *J. Mol. Struct*. **2007**, *827*, 101-107.
[27] James, C.; Amal Raj, A.; Reghunathan, R.; Hubert Joe, I.; Jayakumar, V.S. Structural conformation and vibrational spectroscopic studies of 2,6-bis(p- N, N-dimethyl benzylidene) cyclohexanone using density functional theory. *J. Raman Spectrosc*.**2006**, *37*, 1381-1392.
[28] Luque, F.J.; Lopez, J.M.; Orozco, M. Perspective on Electrostatic interactions of a solute with a continuum. A direct utilization of *ab initio* molecular potentials for the prevision of solvent effects. *Theor. Chem. Acc*. **2000**, *103*, 343-345.
[29] Fleming, I. Frontier Orbitals and Organic Chemical Reactions. Wiley, London, 1976.

[30] Kandemirli, F.; Sagdinc, S. Theoretical study of corrosion inhibition of amides and thiosemicarbazones. *Corros. Sci*. **2007**, *49*, 2118-2130.
[31] Demircioğlu, Z.; Albayrak Kaştaş, Ç..; Büyükgüngör, O.. Theoretical analysis (NBO, NPA, Mulliken Population Method) and molecular orbital studies (hardness, chemical potential, electrophilicity and Fukui function analysis) of (E)-2-((4-hydroxy-2-methylphenylimino)methyl)-3-methoxyphenol. *J. Mol. Struct*. **2015**, *1091*, 183-195.
[32] Gokula Krishnan, K.; Sivakumar, R.; Thanikachalam,V.; Saleem,H.; Arockia doss, M. Synthesis, spectroscopic investigation and computational study of 3-(1-(((methoxycarbonyl)oxy)imino)ethyl)-2H-chromen-2-o ne. *Spectrochim. Acta Part A*. **2015**, *144*, 29-42.
[33] Savithiri, S.; Arockia doss, M.; Rajarajan, G.; Thanikachalam, V.; Bharanidharan, S.; Saleem, H. Spectroscopic (FT-IR, FT-Raman) and quantum mechanical studies of 3t-pentyl-2r,6c-diphenylpiperidin-4-one thiosemicarbazone. *Spectrochim.a Acta Part A*. **2015**, *136*, 782-792.

The author declares no conflict of interest

© 2016 By the Authors; Licensee Borderless Science Publishing, Canada. This is an open access article distributed under the terms and conditions of the Creative Commons Attribution license http://creativecommons.org/licenses/by/3.0